ACS OMEGA

Open Access

http://pubs.acs.org/journal/acsodf

Article

Gelatin Methacryloyl/Sodium Alginate/Cellulose Nanocrystal Inks and 3D Printing for Dental Tissue Engineering Applications

Huihua Li, Shangsi Chen, Waruna Lakmal Dissanayaka,* and Min Wang*

Cite This: *ACS Omega* 2024, 9, 48361−48373

Read Online

ACCESS | Metrics & More | Article Recommendations

ABSTRACT: In tissue engineering, developing suitable printing inks for fabricating hydrogel scaffolds via 3D printing is of high importance and requires extensive investigation. Currently, gelatin methacryloyl (GelMA)-based inks have been widely used for the construction of 3D-printed hydrogel scaffolds and cell-scaffold constructs for human tissue regeneration. However, many studies have shown that GelMA inks at low polymer concentrations had poor printability, and printed structures exhibited inadequate fidelity. In the current study, new viscoelastic inks composed of gelatin methacryloyl (GelMA), sodium alginate (Alg), and cellulose nanocrystal (CNC) were formulated and investigated, with CNC being used to improve the printability of inks and the fidelity of printed hydrogel structures and Alg being used to form ionically cross-linking polymer networks to enhance the mechanical strength of printed hydrogel structures. Rheological results showed that GelMA/Alg/CNC inks with different Alg-to-CNC ratios possessed good shear-thinning behavior, indicating that GelMA/Alg/CNC inks were suitable for 3D printing. The quantitative evaluation of printability and fidelity showed that a high concentration of CNC improved the printability of GelMA/Alg/CNC inks and concurrently promoted the fidelity of printed GelMA/Alg/CNC hydrogels. On the other hand, compression tests showed that a high concentration of Alg could enhance the mechanical strength of GelMA/Alg/CNC hydrogels due to the increase in cross-link density. Furthermore, GelMA/Alg/CNC hydrogels exhibited good biocompatibility and could promote the proliferation of human dental pulp stem cells (hDPSCs), suggesting their great potential in dental tissue engineering.

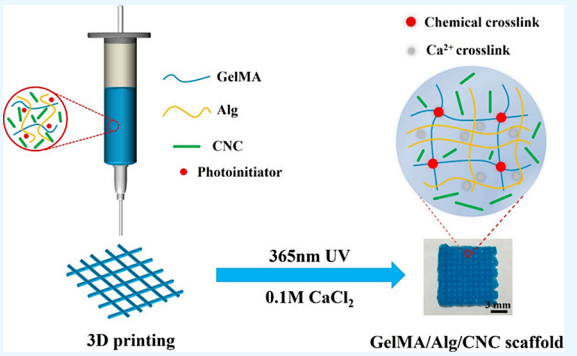

1. INTRODUCTION

Tissue and organ defects caused by trauma, diseases, or aging have always been an inevitable aspect of the human experience, posing an increasingly pressing social problem that jeopardizes both physical and mental well-being of humans.[1,2] Currently, using autografts and allografts is the major treatment for human tissue defects in clinics.[3] However, the shortage of donors, possible disease transmission, and immune rejection have restricted their applications. Therefore, it is essential to develop innovative and promising clinical treatments that can significantly enhance the repair of human tissue. In this context, scaffold-based tissue engineering allows for the creation of three-dimensional (3D) structures that effectively replicate the complex anatomy and functions of targeted tissues. By integrating suitable biomaterials—whether synthetic or natural—with diverse cell types, like mature cells and autologous stem cells, particularly autologous stem cells (which have attracted a lot of attention in recent years), and biomolecules (which play a critical role in directing cell behavior and facilitating the formation of new tissue), this innovative method holds immense promise for the regeneration of human tissues, paving the way for advanced clinical therapies.[4−6] When it comes to scaffold fabrication, traditional methods such as solvent casting/particle leaching, freeze-drying, gas forming, thermal-induced phase separation (TIPS), and electrospinning fall short compared to the advancements offered by 3D printing technologies. The innovative technique allows for the creation of customized, patient-specific scaffolds that closely replicate the intricate anatomical structures of native tissues. This remarkable advantage greatly enhances the prospects for successful tissue repair and regeneration.[7,8]

Among various 3D-printed scaffolds, because of their excellent biocompatibility, tunable biodegradation rate, and good photo-cross-linking ability, gelatin methacryloyl (GelMA) hydrogels have been extensively used for scaffolds to treat many defective tissues, including bone, articular cartilage, dental tissues, blood vessels, skin, and neuron tissues.[9−12] For example, Choi et al. indicated that 3D-printed

Received: July 12, 2024
Revised: October 31, 2024
Accepted: November 13, 2024
Published: November 25, 2024

GelMA-based hydrogels could promote the proliferation and odontoblastic differentiation of human dental pulp stem cells (hDPSCs), showing the potential use for dental applications.[13] Low-concentration GelMA hydrogels are more conducive to cell metabolism and activities. They are therefore efficient for tissue regeneration because of their relatively loose polymer network, high water absorption capacity, and porous structure.[14] However, for extrusion-based 3D printing, the major challenge is that GelMA inks at low GelMA concentrations usually have poor printability. Therefore, the resulting printed hydrogels exhibit inadequate fidelity to the designed 3D structure.[15] In their study, Chen et al. found that 5% GelMA, giving either a high or low degree of methacrylation, provided poor fidelity and insufficient mechanical strength.[16] It is the low concentration of GelMA in printing inks that results in low viscosity and causes instability during printing, which results in poor printability.

Furthermore, the phase transition rate at which low-concentration GelMA hydrogels transform from a liquid to a solid state is insufficient to ensure structural integrity and precision in printed structures, resulting in poor structural fidelity.[17] Another major issue is that low-concentration GelMA hydrogels have insufficient mechanical strength, making them unsuitable for hard tissue regeneration applications. For example, Rizwan et al. discovered that the compression modulus of 15% GelMA hydrogels remained under 50 KPa.[18] O'Connell et al. revealed that the peak storage modulus of 10% GelMA hydrogels was limited to 10 KPa when subjected to high photoinitiator concentrations, light intensity, and prolonged UV exposure.[19]

Many efforts have been made to improve the printability of GelMA inks and enhance the fidelity and mechanical properties of 3D-printed GelMA hydrogels.[17] Generally, other biomaterials, especially natural polymers, are mixed with GelMA to form inks to improve the printing behavior and physiochemical properties of 3D-printed hydrogels.[20,21] For example, cellulose nanocrystals (CNC) have been used to improve the rheological properties of printing inks.[14,22] The addition of CNC could significantly increase the viscosity and promote shear-thinning of GelMA inks, making GelMA-based inks have good printability. Fan et al. showed that CNC could mix with GelMA to form reinforced hydrogel inks and achieve improved printability.[23] Additionally, combining CNC within GelMA could help maintain structural fidelity after 3D printing. On the other hand, the development of double-network (DN) hydrogels has attracted much attention for enhancing the mechanical properties of GelMA-based hydrogels by introducing another cross-linked polymer network in the hydrogels.[24] Sodium alginate (Alg) is a linear polysaccharide with excellent hydrophilicity and histocompatibility. The application of 3D-printed Alg-based hydrogel scaffolds for tissue engineering has been extensively studied due to their excellent biocompatibility and biodegradability, high water content, and similarity to the natural extracellular matrix (ECM).[25,26] Furthermore, Alg-based hydrogels can be cross-linked ionically with divalent cations (e.g., Ca^{2+}) to enhance their mechanical properties. Therefore, GelMA/Alg DN hydrogels containing UV cross-linked covalent and Ca^{2+} cross-linked ionic networks have shown much better mechanical performance than pure GelMA hydrogels.[27]

In the current study, GelMA was mixed with different amounts of Alg and CNC to form reinforced hydrogel inks to improve the printability of the inks and to promote the structural fidelity and mechanical strength of 3D-printed hydrogels (Figure 1). The Alg and CNC concentrations were optimized with regard to ink printability, structural fidelity, and mechanical properties of the reinforced hydrogels. Various experiments were performed to evaluate the new GelMA-based printing inks, and extrusion 3D printing was conducted using these inks. Much improved printability of formulated inks was achieved, and printed scaffolds exhibited enhanced structural fidelity and were promising for dental tissue engineering applications.

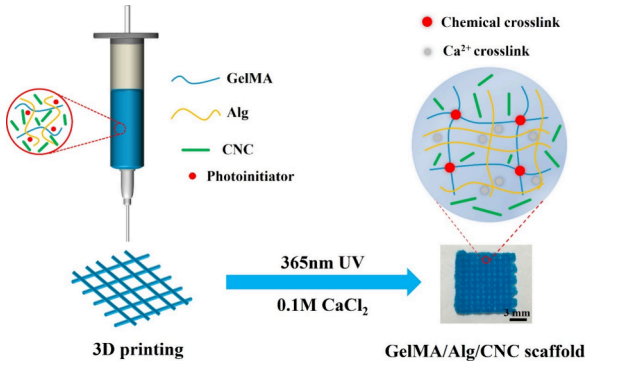

Figure 1. Schematic illustration for 3D printing of GelMA/Alg/CNC scaffolds cross-linked by 365 nm UV light and 0.1 M $CaCl_2$ solution to form double cross-linked hydrogel networks.

2. MATERIALS AND METHODS

2.1. Materials. Gelatin (Gel, type A from porcine skin, powder, gel strength ~300 g Bloom), sodium alginate (viscosity: 5.0−40 cP, 1% in H_2O), methacrylic anhydride (MA, 94%), and 2-hydroxy-2-methylpropiophenone were bought from Sigma-Aldrich. Cellulose nanocrystals (10 nm in width and 200 nm in length) were purchased from Shanghai Macklin Biochemical Co., Ltd. Calcium chloride ($CaCl_2$) was supplied by Uni Chem Co., Korea. The dialysis tubing cellulose membrane (MWCO 10 kDa) was obtained from Thermo Fisher Scientific. All reagents were utilized as received without further purification.

2.2. Synthesis of GelMA. GelMA was synthesized following the procedure as described in previous studies.[16,28] Briefly, 10 g of Gel was dissolved in 100 mL of phosphate-buffered saline (PBS) at 50 °C, maintaining constant magnetic stirring for 1 h. Subsequently, 0.8 mL of MA was added dropwise to the gelatin solution. After the mixture was reacted for 3 h, five times the volume of PBS was introduced to effectively stop the reaction. Then, the mixture was transferred into dialysis tubing and dialyzed against deionized (DI) water at 40 °C for 1 week with DI water being refreshed daily. Finally, GelMA was obtained by freeze-drying and then was stored at 4 °C for further use. The degree of substitution of GelMA was characterized by ^{1}H NMR spectroscopy (Bruker Avance III 400). The secondary structure of GelMA was investigated by a circular dichroism (CD) spectrometer (JASCO J-815, Japan) at 4, 20, and 37 °C. Furthermore, the functional groups of GelMA were studied using an FT-IR spectrometer (PerkinElmer) under the attenuated total reflection (ATR) mode.

2.3. Preparation of GelMA/Alg/CNC inks. GelMA/Alg/CNC printing inks were prepared as follows. Briefly, 10% (*w*/*v*) GelMA solutions were prepared by dissolving GelMA in

https://doi.org/10.1021/acsomega.4c06458
ACS Omega 2024, 9, 48361−48373

PBS at 40 °C using a water bath under constant magnetic stirring. Six ink formulations were prepared by having different Alg: CNC mass ratios, namely, 0:5, 1:4, 2:3, 3:2, 4:1, and 5:0, with a total solid content of 5% (w/v) for a final volume of 5 mL, to GelMA solutions. A photoinitiator (2-hydroxy-2-methylpropiophenone) was added to each ink with a final concentration of 0.2% (*w/v*).The final concentration of each component in the different inks is listed in Table 1. The six printing inks having different concentrations of Alg and CNC were designated as GelMA-0A5C, GelMA-1A4C, GelMA-2A3C, GelMA-3A2C, GelMA-4A1C, and GelMA-5A0C.

Table 1. Concentrations (%) of GelMA, Alg, and CNC in Different Printing Inks

	GelMA (w/v)	Alg (w/v)	CNC (w/v)	photoinitiator (w/v)
GelMA-0A5C	10	0	5	0.2
GelMA-1A4C	10	1	4	0.2
GelMA-2A3C	10	2	3	0.2
GelMA-3A2C	10	3	2	0.2
GelMA-4A1C	10	4	1	0.2
GelMA-5A0C	10	5	0	0.2

2.4. Rheological Properties of GelMA/Alg/CNC Inks. The rheological properties of GelMA/Alg/CNC inks were characterized at 20 °C using a rotational rheometer (MCR302, Anton Paar, Austria) equipped with a parallel plate unit with a 25 mm diameter and a 0.5 mm measurement gap. The shear-thinning phenomenon of the inks was investigated at a shear rate from 0.1 to 100 s^{-1}. The viscosity results of the inks were calculated according to the power law model:[29]

$$\eta = K\gamma^{(n-1)} \tag{1}$$

where η is the shear viscosity (Pa·s) of inks, K is the consistency index (Pa·s), γ is the shear rate (s^{-1}), and n is the flow index of inks.

The thixotropic behavior of GelMA/Alg/CNC inks was investigated by repetitive application of shear rates of 0.1 s^{-1} for 120 s and 100 s^{-1} for 60 s. Moreover, based on the preliminary strain sweep test results, the storage moduli (G') and loss moduli (G'') of GelMA/Alg/CNC inks subjected to a maximum strain (γ) of 1.0% were measured at a frequency range of 0.1−100 rad/s. The G' and G'' of GelMA/Alg/CNC hydrogels with UV light cross-linking and Ca^{2+} cross-linking were also studied at a frequency range of 0.1−100 rad/s.

The thixotropic behavior of GelMA/Alg/CNC inks was assessed by applying shear rates of 0.1 s^{-1} for 120 and 100 s^{-1} for 60 s. Preliminary strain sweep tests showed that the storage moduli (G') and loss moduli (G'') of the inks, subjected to a maximum strain (γ) of 1.0%, were measured across a frequency range of 0.1−100 rad/s. Additionally, the G' and G'' of GelMA/Alg/CNC hydrogels, both subjected to UV light cross-linking and Ca^{2+} cross-linking, were investigated within the same frequency range.

2.5. 3D Printing of Hydrogel Structures. 3D printing of GelMA/Alg/CNC hydrogels was conducted by using a 3D bioprinter (3D Discovery Evolution, regenHU Ltd., Switzerland). GelMA/Alg/CNC inks were loaded into a syringe dispenser and installed on the 3D bioprinter. Printing was conducted at a temperature of 20 °C, with a nozzle inner diameter of 0.26 mm and a printing speed adjusted to the ink extrusion rate. Following the 3D printing process, the GelMA/Alg/CNC hydrogels underwent UV irradiation (365 nm) for 5 min to facilitate the cross-linking of the GelMA polymer chains. The printed hydrogels were then immersed in a 0.1 M $CaCl_2$ solution for 1 h for alginate cross-linking. Finally, the GelMA/Alg/CNC hydrogels were freeze-dried and then stored at 4 °C for subsequent use.

2.6. Characterization and Evaluation of 3D-Printed Hydrogels. *2.6.1. Printability of Inks and Structural Fidelity of Printed Hydrogels.* The printability (Pr) of GelMA/Alg/CNC inks was assessed by using ImageJ software, measuring the area and perimeter of interconnected pores right after 3D printing. The Pr value was derived from the following formula:[30]

$$\mathrm{Pr} = \frac{L^2}{16A} \tag{2}$$

where Pr is the printability value of GelMA/Alg/CNC inks, L is the perimeter of the printed pore, and A is the area of the pore in the printed hydrogel.

The structural fidelity of the printed GelMA/Alg/CNC hydrogels was analyzed using ImageJ software to calculate the expansion percentage of the printed strut compared to the designed strut width immediately after 3D printing. It was calculated according to the following formula:

$$\text{Strut expansion percentage} = \frac{(D_1 - D_0)}{D_0} \times 100\% \tag{3}$$

where D_1 is the width of the printed struts of the GelMA/Alg/CNC hydrogels, and D_0 is the width of the designed struts of the GelMA/Alg/CNC hydrogels.

2.6.2. Morphology and Structure of 3D-Printed Hydrogels. The morphology of 3D-printed GelMA/Alg/CNC hydrogels with different ratios of Alg:CNC was observed by using a field emission scanning electron microscope (Hitachi S4800 SEM, Japan). Lyophilized GelMA/Alg/CNC hydrogel samples were sputter-coated with a thin layer of gold. The gold-coated hydrogel samples were then examined under SEM. Furthermore, the phase structure of hydrogel samples was studied using an X-ray diffractometer (XRD, 7000S, Shimadzu, Japan) over a range of 2θ from 5° to 60°. Thermogravimetric analysis (TGA) was conducted using a thermogravimetric analyzer (TA Instruments Q50 TGA) to determine the component percentage of the GelMA/Alg/CNC hydrogel samples.

2.6.3. Mechanical Properties of GelMA/Alg/CNC Hydrogels. The mechanical properties of the GelMA/Alg/CNC hydrogels cross-linked by UV light and a $CaCl_2$ solution were assessed through compression tests. Wet cylindrical hydrogel samples of 10 mm in diameter and 10 mm in height were made and then tested in compression at a 1.0 mm/min testing speed using a universal mechanical testing machine (Model 5848, Instron Ltd.). The ultimate compression strength of the GelMA/Alg/CNC hydrogels was calculated by dividing the maximum load at breakage by the original cross-sectional area. The compressive modulus of the GelMA/Alg/CNC hydrogels was derived from the slope of the initial linear section of stress−strain curves. Furthermore, cyclic compression tests were performed by compressing the hydrogel samples to 30% strain and then reversing at the same testing speed (i.e., 1.0 mm/min). The hysteresis in each stress−strain curve was recorded and compared.

https://doi.org/10.1021/acsomega.4c06458
ACS Omega 2024, 9, 48361−48373

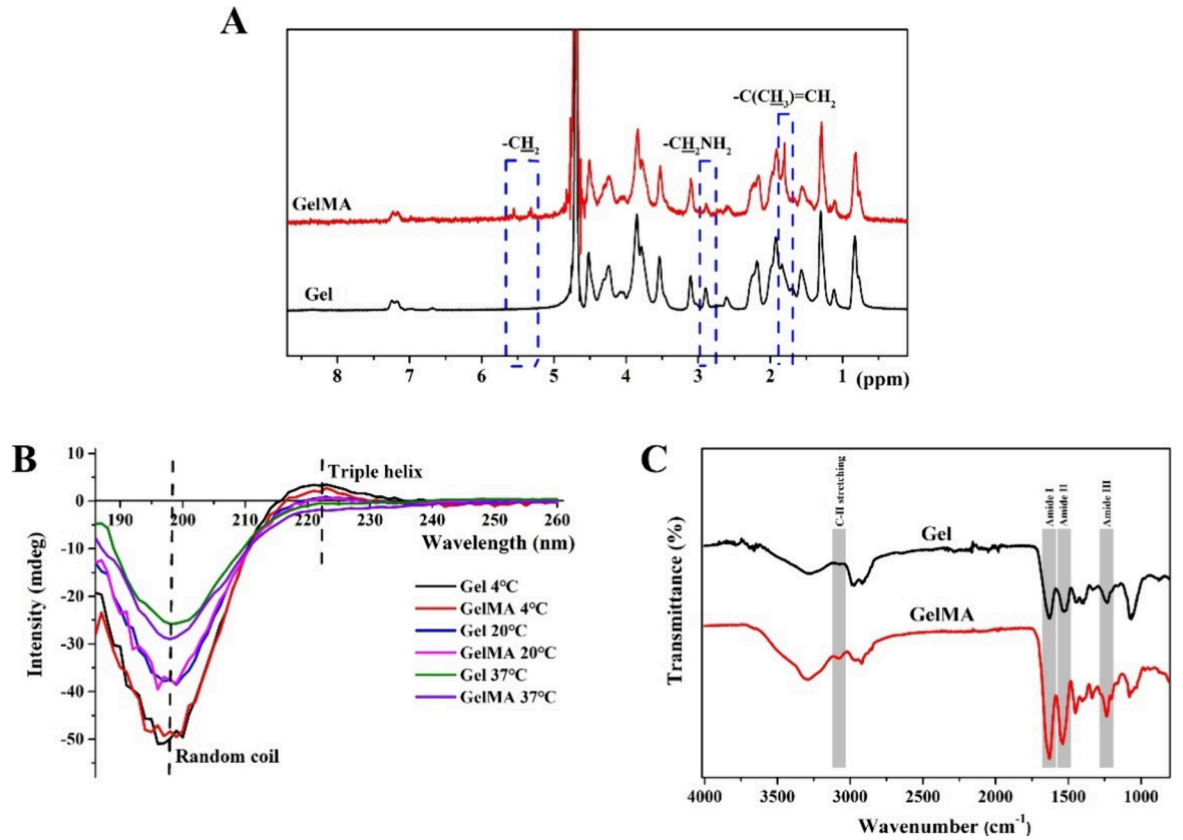

Figure 2. Characteristics of GelMA molecules in comparison with Gel. (A) ^{1}H NMR spectra, (B) CD, and (C) FT-IR spectra.

2.6.4. Swelling Behavior and In Vitro Degradation of GelMA/Alg/CNC Hydrogels. To investigate the dynamic swelling behavior, lyophilized hydrogel samples were weighed and recorded as W_0. Subsequently, lyophilized hydrogel samples were immersed in PBS at 37 °C. At each predetermined time interval, GelMA/Alg/CNC hydrogel samples were taken out, and excess PBS on the surfaces of samples was gently blotted away. The weight of swollen GelMA/Alg/CNC hydrogel samples was measured as W_1. The swelling ratio of GelMA/Alg/CNC hydrogels was calculated using the following formula:

$$\text{Swelling ratio} = \frac{(W_1 - W_0)}{W_0} \times 100\% \quad (4)$$

To investigate the in vitro degradation behavior of GelMA/Alg/CNC hydrogels, the weight of each dried hydrogel sample was measured as M_0. Then, the dry hydrogel samples were immersed in 5 mL of PBS containing 0.02% sodium azide (NaN_3) and placed in a shaking water bath at 37 °C. The immersion liquid was changed every 2 days. At each designated time point, hydrogel samples were taken out and freeze-dried to measure their postdegradation weight, noted as M_1. The degradation rate of GelMA/Alg/CNC hydrogels was obtained using the following formula:

$$\text{Degradation rate} = \frac{(M_0 - M_1)}{M_0} \times 100\% \quad (5)$$

2.7. In Vitro Biological Performance of GelMA/Alg/CNC Hydrogels. Human dental pulp stem cells (hDPSCs), sourced from Lonza (Basel, Switzerland) at passages 3−8, were cultured in α-MEM (Minimum Essential Medium α, Gibco, Thermo Fisher Scientific, USA) supplemented with 10% (v/v) fetal bovine serum (FBS, Gibco, Thermo Fisher Scientific, USA) and 1% (v/v) penicillin/streptomycin (PS, Gibco, Thermo Fisher Scientific, USA) in a CO_2 incubator at 37 °C. Dried hydrogel samples were sterilized using ^{60}Co γ-irradiation with an intensity of 15 kGy for 30 min and then put into a 48-well plate. Subsequently, the cell-free culture medium was added to facilitate cell attachment to the sample surface. hDPSCs at a density of 2×10^3 cells per well were seeded on GelMA/Alg/CNC hydrogel samples. Then, the cell-seeded hydrogel samples were incubated in a CO_2 incubator at 37 °C with 5% CO_2. The culture medium was refreshed every 2 days.

The cell survival rate of hDPSCs cultured on the hydrogel samples was determined using a live/dead assay. After culturing for 24 and 72 h, respectively, 200 μL of live/dead staining working solution consisting of calcein-AM (2 μM, Invitrogen, Thermo Fisher Scientific, USA) and EthD-1 (4 μM, Invitrogen, Thermo Fisher Scientific, USA) was added to immerse cell-hydrogel samples for 30 min in the dark at room temperature. Afterward, the samples were observed under a fluorescence microscope (Leica, DMi8, Germany). The hDPSCs proliferation rate on GelMA/Alg/CNC hydrogels was evaluated using MTT ((3-[4,5-dimethylthiazol-2-yl]-2,5 diphenyl tetrazolium bromide)) tests. Briefly, hDPSCs at a density of 1×10^3 cells per well were seeded on GelMA/Alg/CNC hydrogel samples in a 48-well plate. After the cells were cultured for 1, 3, and 7 days, cell viability was measured using the MTT assay.

2.8. Statistical Analysis. The results presented in this study were derived from at least three separate samples or tests and are expressed as the mean ± standard deviation (SD). One-way analysis of variance (ANOVA) was conducted for

https://doi.org/10.1021/acsomega.4c06458
ACS Omega 2024, 9, 48361−48373

statistical analysis. Statistically significant difference was indicated by *p < 0.05, **p < 0.01, ***p < 0.001, and ****p < 0.0001.

3. RESULTS AND DISCUSSION

3.1. Synthesis and Characteristics of GelMA. Gelatin (Gel) has been a popular biomaterial for extrusion-based 3D printing because of its thermoresponsive behavior. At lower temperatures, it transforms into a solid hydrogel driven by the formation of a partial triple-helix structure. When subjected to higher temperatures, it shifts to an aqueous state due to the formation of a random coil structure.[31,32] Notably, the transformation from a triple helix to a random coil is reversible. Although 3D-printed Gel-based hydrogels have been used for tissue engineering applications, some intrinsic limitations, i.e., insufficient mechanical strength and an uncontrollable degradation rate, must be tackled for its wider use.[33] Given that Gel has many active side chains (e.g., $-NH_2$), Gel can react with MA to form photocurable GelMA molecules by methacrylation of the lysine groups in Gel polymer chains. Consequently, GelMA is similar to Gel with regard to its biocompatibility, biodegradability, and the presence of Arg-Gly-Asp (RGD) sequences for promoting cell attachment. Although introducing methacrylate groups may interfere with the secondary structure of Gel molecules, previous studies have shown that GelMA with a suitable degree of substitution of the methacrylate groups could also be thermoresponsive.[16] Furthermore, compared to Gel, GelMA can be covalently cross-linked by a water-soluble photoinitiator to form a stable structure when irradiated by UV light, which can significantly improve the mechanical strength of GelMA hydrogels. Therefore, due to its thermoresponsive and photocurable ability, GelMA has been extensively used to create various hydrogel structures for tissue engineering via 3D printing.[34,35]

In the current study, GelMA was synthesized in PBS by grafting methacrylate functional groups onto the Gel backbone using the reactions between MA and lysine residues. The ^{1}H NMR spectra shown in Figure 2A indicated that new peaks around 6.00−5.86 ppm (m, $-O-CH_2-CH=CH_2$) and 5.38−5.22 ppm (t, $-O-CH_2-CH=CH_2$) appeared in GelMA polymer chains. Furthermore, the heightened intensity of the methyl peak at ∼1.8 ppm, combined with the diminished intensity of the lysine methylene peak at 2.8−3.0 ppm, further indicated the successful incorporation of the methacrylate groups in GelMA. Moreover, the degree of substitution of GelMA was determined to be ∼20% after calculations from the ^{1}H NMR spectra and 2,4,6-trinitrobenzenesulfonic acid (TNBS) assays. The CD spectra shown in Figure 2B indicated that the methacryloylation of GelMA in this study might affect the secondary structure of Gel. As shown in Figure 2B, the intensity at 198 nm is attributed to the random coil structure formation, and the intensity at 223 nm is due to the formation of a triple-helix structure. Table 2 shows that Gel exhibited a higher intensity at 223 nm at 4 and 20 °C than GelMA, suggesting that the formation of methacrylate groups in GelMA chains could influence the secondary structure of GelMA and the interactions among GelMA polymer chains and therefore weaken the thermoresponsive ability of GelMA. Moreover, the intensities at 223 nm at 4 and 20 °C of GelMA are 2.69 and 0.49, respectively, indicating that GelMA solutions could form a Gel state at 4 and 20 °C. Furthermore, the FT-IR spectra shown in Figure 2C indicated that GelMA preserved the characteristic peaks of the Gel polymer chains at 1645 cm^{-1} (amide I), 1526 cm^{-1} (amide II), and 1240 cm^{-1} (amide III). Additionally, due to the introduction of the methacrylate groups in GelMA, the intensity of C−H stretching at 3284 cm^{-1} increased.

Table 2. Peak Intensity at 198 and 223 nm in CD Spectra of GelMA and Gel at 4, 20, and 37 °C

	intensity					
	4 °C		20 °C		37 °C	
material	198 nm	223 nm	198 nm	223 nm	198 nm	223 nm
GelMA	−48.39	2.69	−37.62	0.49	−28.97	−1.97
Gel	−49.88	3.45	−37.48	0.89	−28.97	−1.97

3.2. Rheological Properties of GelMA/Alg/CNC Inks. As discussed in the Introduction, GelMA inks at low concentrations exhibited poor printability. Therefore, to improve the printability of GelMA inks, Alg and CNC at different ratios were added to GelMA solutions to form GelMA/Alg/CNC inks. For extrusion-based 3D printing, the viscosity of inks is paramount for achieving good extrudability.[36] If the viscosity is excessively low, inks can easily leak from the nozzle of the printing head, making it difficult to maintain the structural stability of the printed hydrogels. Alternatively, overly high viscosity leads to a semisolid state, necessitating high pressures for extrusion or even preventing the inks from being extruded.[37] Thus, an ideal printing ink must showcase shear-thinning behavior, like non-Newtonian fluids, decreasing in viscosity as the shear rate increases.[38]

The rheological properties of GelMA/Alg/CNC inks with different Alg:CNC ratios were investigated by using shear rate sweep tests. As shown in Figure 3A, the six GelMA/Alg/CNC ink formulations showcased remarkable shear-thinning behavior as the shear rate increased from 0.1 to 100 s^{-1}. The viscosity increase of GelMA/Alg/CNC inks was more pronounced with an increase in Alg content than with an increase in CNC content. For example, the GelMA-5A0C ink showed a much higher viscosity than the GelMA-0A5C ink, which was attributed to the high viscosity of the Alg solution in comparison to the CNC solution. Moreover, the viscosity curves of different GelMA/Alg/CNC inks were adjusted to the power law model to examine the extent of the shear-thinning behavior. It should be noted that the fluid index (n) determines the rheology of a fluid.[39] If $0 < n < 1$, the fluid is non-Newtonian and exhibits shear-thinning behavior. In the current study, as shown in Figure 3B, the n value of all GelMA/Alg/CNC inks was lower than 1 and was in the low fractions of 1 (0.155 ± 0.023 for GelMA-0A5C ink, 0.184 ± 0.002 for GelMA-1A4C ink, 0.223 ± 0.010 for GelMA-2A3C ink, 0.258 ± 0.008 for GelMA-3A2C ink, 0.293 ± 0.017 for GelMA-4A1C ink, and 0.295 ± 0.024 for GelMA-5A0C ink), suggesting good shear-thinning behavior. Subsequently, the thixotropic behavior of GelMA/Alg/CNC inks was studied through the repeated application of a low shear rate (0.1 s^{-1}) for 120 s and a high shear rate (100 s^{-1}) for 60 s [Figure 3C]. The six GelMA/Alg/CNC inks all exhibited excellent thixotropic behavior. These results suggested that the six GelMA/Alg/CNC inks could be easily extruded from the printing head nozzle, making them suitable for the application for extrusion-based 3D printing.

G' and G'' reflect the elastic and viscous properties of a material. The rheological properties of GelMA/Alg/CNC inks without and with cross-linking were determined through

https://doi.org/10.1021/acsomega.4c06458
ACS Omega 2024, 9, 48361−48373

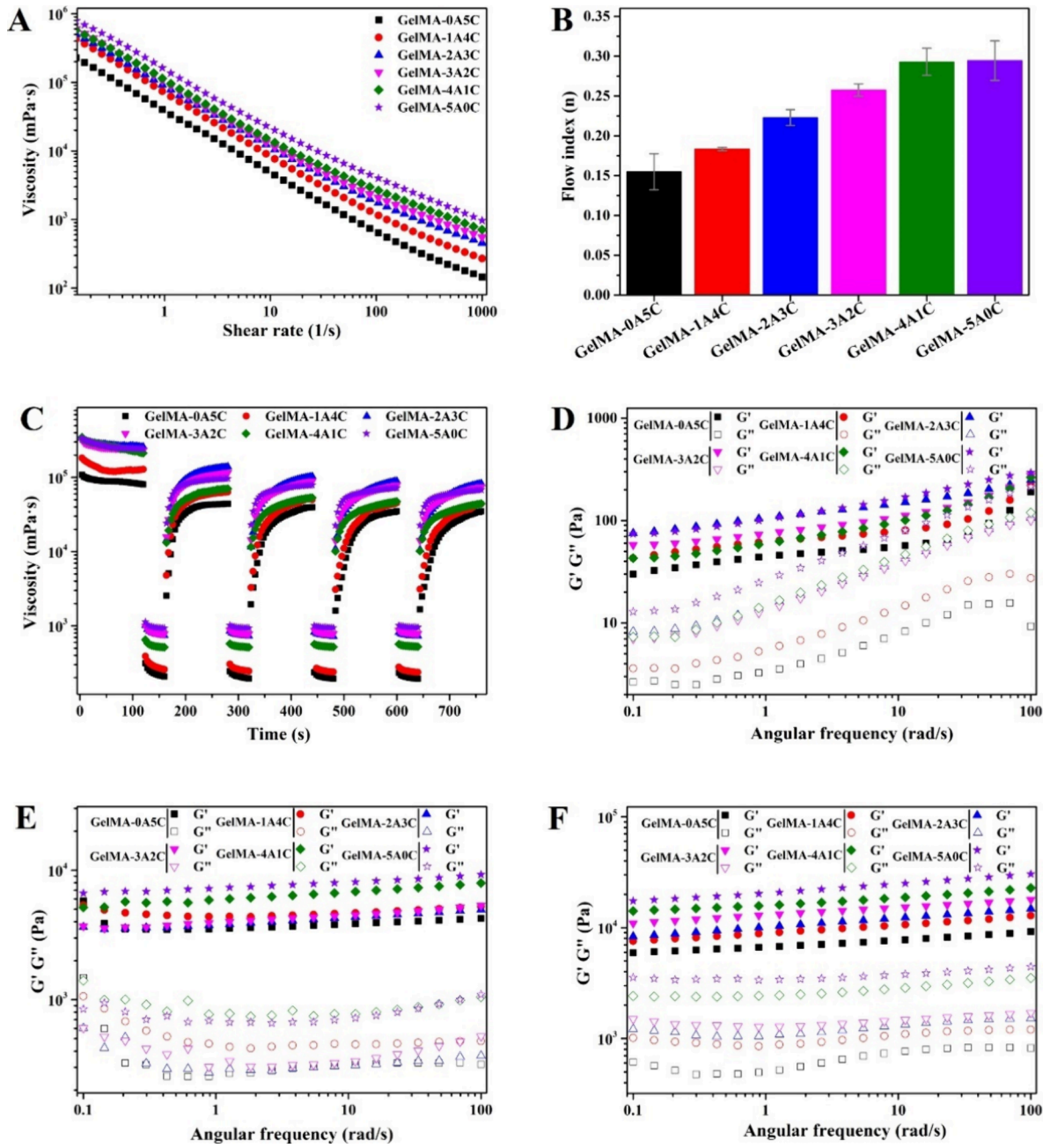

Figure 3. Rheological properties of GelMA/Alg/CNC inks: (A) shear-thinning behavior, (B) fluid index values, and (C) thixotropic behavior; and frequency sweep curves of (D) GelMA/Alg/CNC inks without cross-linking, (E) GelMA/Alg/CNC inks cross-linked by UV light, and (F) GelMA/Alg/CNC inks cross-linked by UV light and $CaCl_2$ solution.

frequency sweep tests. As shown in Figure 3D, the G' value of GelMA/Alg/CNC inks without cross-linking was higher than G'' at 20 °C, suggesting the elastic state of inks. It might be attributed to the 10% (w/v) GelMA. Previous studies indicated that 10% (w/v) GelMA inks could be in a gel state at room temperature.[40] After being exposed to UV light, the G' and G'' values of GelMA/Alg/CNC inks dramatically increased [Figure 3E], which was due to cross-linking of GelMA chains, forming robust GelMA/Alg/CNC hydrogels. Furthermore, after being immersed in the $CaCl_2$ solution to form DN hydrogels, the G' and G'' values of GelMA/Alg/CNC hydrogels became much higher than those with UV light cross-linking only [Figure 3F]. Notably, GelMA-5A0C gave the highest value for G'.

3.3. Structure and Properties of GelMA/Alg/CNC Hydrogels. *3.3.1. Printability of Inks and Fidelity of 3D-Printed Hydrogels.* Printability is an important factor for evaluating the suitability of inks or bioinks for 3D printing/bioprinting.[41,42] It refers to the ability of a printing ink to be printed continuously and consistently and to form stable 3D structures according to the design during and after printing. It can affect the physical properties (e.g., pore shape, pore size, and porosity) of printed structures and, therefore, can determine the mechanical properties and biological performance of printed structures.[43] In the current study, the pore shape formed after 3D printing was used to assess the printability of GelMA/Alg/CNC inks. A Pr value close to 1 indicates excellent printability of the printing ink.[30] Figure 4A

https://doi.org/10.1021/acsomega.4c06458
ACS Omega 2024, 9, 48361−48373

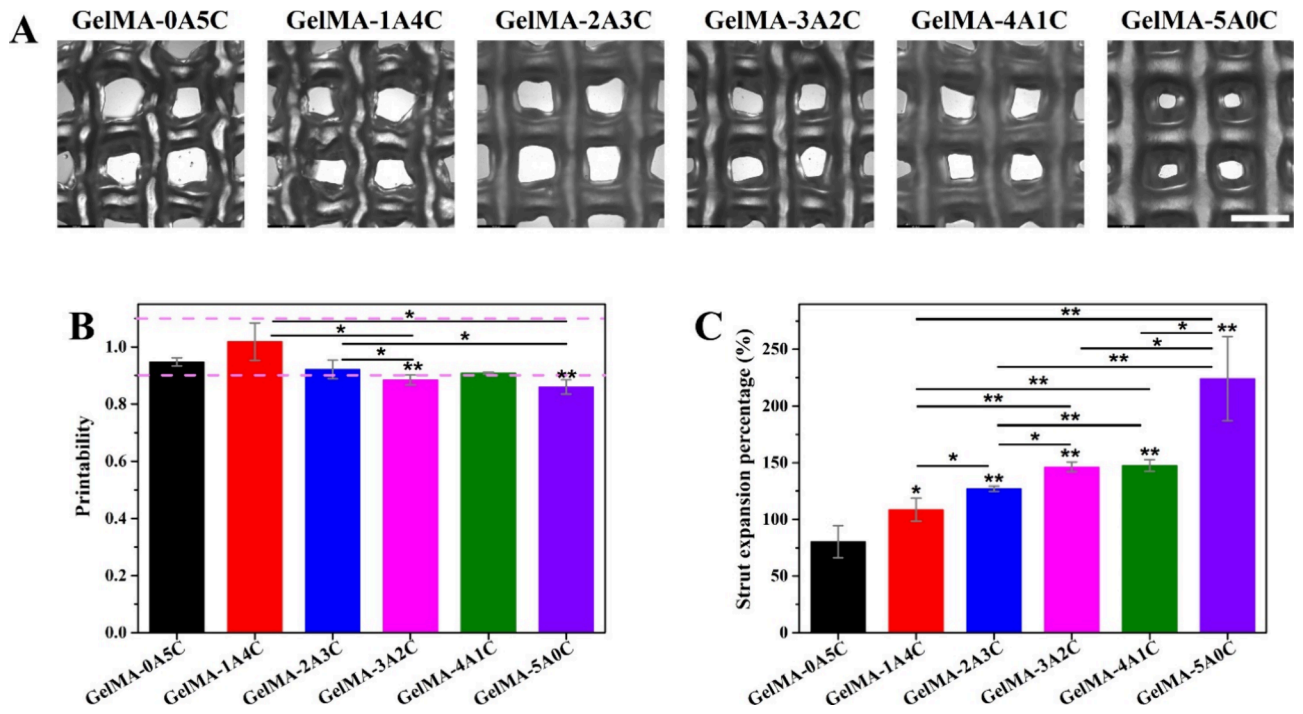

Figure 4. Printability of GelMA/Alg/CNC inks and fidelity of 3D-printed GelMA/Alg/CNC hydrogels: (A) optical images of 3D-printed GelMA/Alg/CNC hydrogels. Scale bar: 1 mm. (B) Printability of GelMA/Alg/CNC inks. (C) Strut expansion percentage of GelMA/Alg/CNC hydrogels.

shows optical images of the morphology and structure of GelMA/Alg/CNC hydrogels after 3D printing, and Figure 4B gives Pr values of GelMA/Alg/CNC inks. Typically, inks with a Pr value in the range of 0.9−1.1 are recognized to have good printability and be able to maintain the pore shape. As shown in Figure 4B, the Pr values of GelMA-0A5C, GelMA-1A4C, and GelMA-2A3C inks were within the range of 0.9−1.1, suggesting their good printability, which is better than the printability of 10%Gel + 1%Alg inks used in a previous study.[30] Moreover, the addition of CNC made the printability of GelMA/Alg/CNC inks better than Gel/GelMA inks.[44] The Pr values of GelMA-3A2C, GelMA-4A1C, and GelMA-5A0C inks, which had high Alg concentrations but low CNC concentrations, were just below 0.9, indicating their relatively poor printability.

Fidelity is said to be the ability to maintain the structure of printed objects.[45,46] It is a commonly used index for assessing how similar the structure of printed objects is to that of the design. Poor fidelity in printed structures often arises from the deformation of printed struts, leading to an increase in the width and a decrease in the thickness. Therefore, in the current study, the degree of expansion of printed struts was used to evaluate the fidelity of the printed hydrogels. As shown in Figure 4C, the GelMA-0A5C hydrogel had the lowest strut expansion percentage (80.31 ± 14.09%), and the GelMA-5A0C hydrogel exhibited the highest strut expansion percentage (224.20 ± 37.23%). The results indicated that GelMA/Alg/CNC hydrogels with high concentrations of CNC could provide good fidelity, while hydrogels with high concentrations of Alg would offer low fidelity. Overall, a high concentration of CNC in the ink could improve the printability of GelMA/Alg/CNC inks and the fidelity of 3D-printed GelMA/Alg/CNC hydrogels.

3.3.2. Morphology and Structure of 3D-Printed Hydrogels. Figure 5 shows the surface morphology and microstructure of dried 3D-printed GelMA/Alg/CNC hydrogels after cross-linking by UV light and $CaCl_2$ solution to form double-cross-linked hydrogel networks. These SEM images indicated that all GelMA/Alg/CNC hydrogel scaffolds had smooth strut surfaces. It should be noted that the difference in Alg:CNC ratios did not affect the surface morphology of GelMA/Alg/CNC hydrogel scaffolds. Moreover, all GelMA/Alg/CNC hydrogel scaffolds retained interconnected structures after double cross-linking, which is beneficial for cell metabolism and activities, i.e., cell adhesion, proliferation, and differentiation, by creating channels that effectively transport oxygen and essential nutrients to attached and/or encapsulated cells.[47]

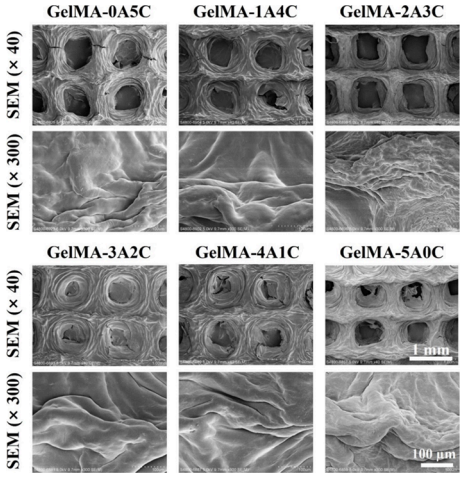

Figure 5. SEM images showing the surface morphology and microstructure of 3D-printed GelMA/Alg/CNC hydrogels.

As shown in Figure 6A, GelMA/Alg/CNC hydrogel scaffolds had characteristic peaks of GelMA, Alg, and CNC. XRD patterns displayed in Figure 6B indicated that GelMA

https://doi.org/10.1021/acsomega.4c06458
ACS Omega 2024, 9, 48361−48373

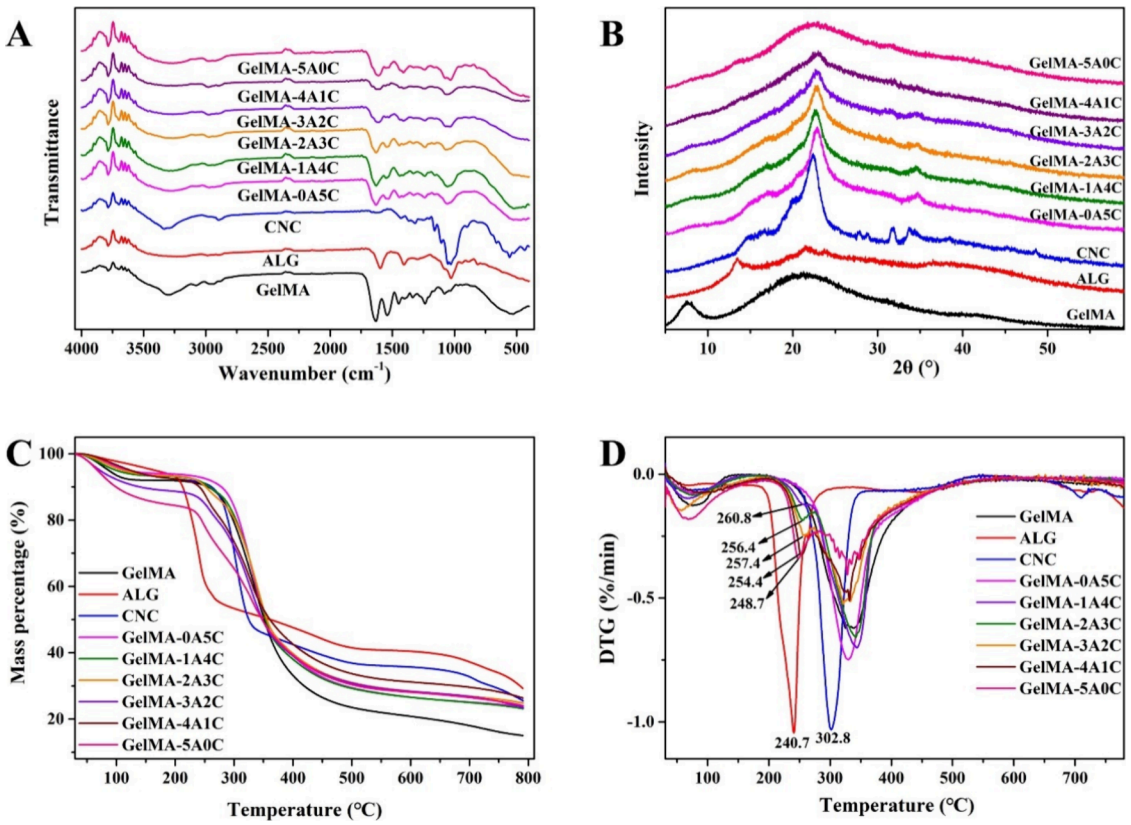

Figure 6. Results of different analyses for GelMA/Alg/CNC hydrogels: (A) FT-IR spectra, (B) XRD patterns, (C) TG curves, and (D) DTG analysis.

had a peak at 20−25°, which was attributed to the triple-helix structure.[48] Additionally, CNC displayed the characteristics peaks of cellulose I at 15.2°, 16.6°, 22.4° and 34.4°, which corresponded to (110), (101), (200), and (004) planes of cellulose I, respectively.[49] The GelMA-5A0C hydrogel exhibited a characteristic peak of the triple-helix structure at 20−25°, while other GelMA/Alg/CNC hydrogels showed the characteristic cellulose I peak of the (200) plane. Moreover, with a high concentration of CNC, GelMA/Alg/CNC hydrogels exhibited high intensity of the cellulose I peak of the (200) plane. In Figure 6C, TGA analysis showed the thermal degradation behavior of GelMA/Alg/CNC hydrogels. It was found that CNC had the fastest decomposition rate at 302.8 °C, while Alg had the fastest decomposition rate at 240.7 °C (Figure 6D). With the increase in Alg concentration, the fastest decomposition temperature of GelMA-1A4C, GelMA-2A3C, GelMA-3A2C, GelMA-4A1C, and GelMA-5A0C hydrogels shifted to 260.8, 256.4, 257.4, 254.4, and 248.7 °C, respectively.

3.3.3. Mechanical Properties of GelMA/Alg/CNC Hydrogels. The mechanical properties of wet GelMA/Alg/CNC hydrogels with different Alg:CNC ratios were investigated through compression tests. Figure 7A displays typical stress−strain curves of the GelMA/Alg/CNC hydrogels. As shown in Figure 7B, the compressive moduli of GelMA-0A5C, GelMA-1A4C, GelMA-2A3C, GelMA-3A2C, GelMA-4A1C, and GelMA-5A0C hydrogels were 34.07 ± 2.70, 57.66 ± 3.14, 90.17 ± 7.73, 110.65 ± 11.45, 128.96 ± 22.13, and 128.07 ± 12.30 KPa, respectively. The compressive modulus of GelMA/Alg/CNC hydrogels was much higher than the compressive modulus of GelMA/cellulose nanofibrils (CNF) hydrogels, which was in the range of 2.3−4.5 kPa, as reported in a previous study.[14] It was noted that GelMA/Alg/CNC hydrogels with a high concentration of Alg exhibited a higher compressive modulus, which was attributed to the formation of double cross-linking hydrogel networks. Increasing the amount of Alg in GelMA/Alg/CNC hydrogels would increase the cross-link density and thus could make the hydrogel more robust.[27,50] Moreover, the ultimate compressive strengths of GelMA-0A5C, GelMA-1A4C, GelMA-2A3C, GelMA-3A2C, GelMA-4A1C, and GelMA-5A0C hydrogels were 61.16 ± 6.01, 98.66 ± 7.02, 184.51 ± 16.25, 241.80 ± 40.97, 249.4 ± 10.46, and 208.33 ± 18.99 KPa, respectively [Figure 7C]. The compression strains of GelMA-0A5C, GelMA-1A4C, GelMA-2A3C, GelMA-3A2C, GelMA-4A1C, and GelMA-5A0C hydrogels were 58.19 ± 1.39, 57.72 ± 3.58, 58.56 ± 2.53, 57.14 ± 3.24, 52.74 ± 1.11, and 52.54 ± 2.35%, respectively [Figure 7D], suggesting the high elastic properties of all six GelMA/Alg/CNC hydrogels. Importantly, the increase of the Alg amount, which increased the cross-link density in GelMA/Alg/CNC hydrogels, had little effect on the compression strain. The results of cyclic compression tests shown in Figure 8 indicate that all GelMA/Alg/CNC hydrogels in the wet state with different Alg:CNC ratios had good elasticity and also good recovery after being compressed to 30% strain. However, with the increase in Alg amount and decrease in CNC amount, the ultimate mechanical strength increased together with larger hysteresis.

3.3.4. Swelling Behavior and In Vitro Degradation Behavior of GelMA/Alg/CNC Hydrogels. The swelling characteristic of hydrogels is important for the diffusion and migration of small biomolecules, drugs, and cells encapsulated

https://doi.org/10.1021/acsomega.4c06458
ACS Omega 2024, 9, 48361−48373

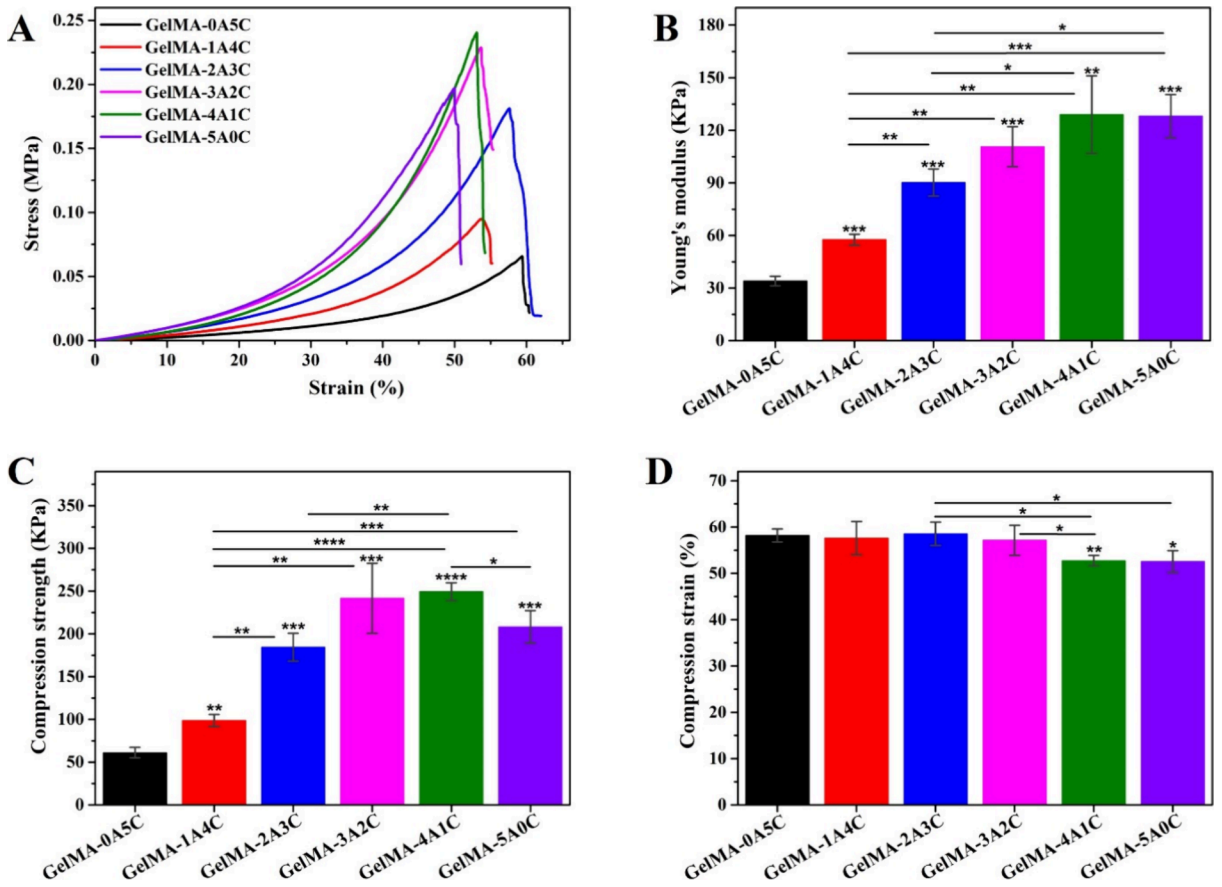

Figure 7. Mechanical properties of GelMA/Alg/CNC hydrogels in the wet state: (A) compressive stress−strain curves, (B) compressive modulus, (C) compression strength, and (D) compression strain.

within them. It plays an important role in cell survival and growth.[51] In addition, swelling capacity is an important feature of hydrogels, which is linked to structural integrity and dimensional stability, as hydrogels tend to swell upon interactions with biological fluids, changing their weight and size.[52] The swelling behavior of GelMA/Alg/CNC hydrogels was investigated by immersing dry hydrogel samples in PBS for up to 96 h in a water bath at 37 °C. As shown in Figure 9(A), the swelling curves of GelMA/Alg/CNC hydrogels illustrated that almost all hydrogels reached their swelling equilibrium after immersion for 24 h. The swelling ratios of GelMA-0A5C, GelMA-1A4C, GelMA-2A3C, GelMA-3A2C, GelMA-4A1C, and GelMA-5A0C hydrogels were 613.40 ± 35.26, 586.41 ± 13.04, 526.87 ± 33.45, 656.01 ± 148.89, 872.11 ± 60.05, and 1014.44 ± 180.39%, respectively. It was noted that the swelling ratio of GelMA/Alg/CNC hydrogels increased as the concentration of Alg increased, which was similar to findings in previous studies.[24] Because Alg has an excellent water absorption ability, adding Alg in GelMA-based hydrogels could improve the swelling behavior and significantly increase the swelling ratio.

The in vitro or in vivo degradation of a hydrogel scaffold could facilitate the formation of an ECM and, therefore, create an optimal microenvironment for cell proliferation.[53] Moreover, the biodegradation rate of hydrogels should be in line with the rate at which new tissue is formed. In the current study, to investigate the degradation behavior of double-cross-linked GelMA/Alg/CNC hydrogels, hydrogel samples were cultured in PBS at 37 °C for over 2 weeks. As shown in Figure 9B, the GelMA-0A5C hydrogel exhibited the lowest degradation rate, while GelMA-5A0C and GelMA-4A51 hydrogels had relatively high degradation rates. After culturing for 2 weeks, the degradation rates of GelMA-0A5C, GelMA-1A4C, GelMA-2A3C, GelMA-3A2C, GelMA-4A1C, and GelMA-5A0C hydrogels were 35.50 ± 3.22, 40.54 ± 2.33, 38.85 ± 2.41, 43.17 ± 3.14, 49.27 ± 7.80, and 45.25 ± 1.47%, respectively. Increasing the Alg content contributed to higher biodegradation. This could be explained by the easy disintegration of Ca^{2+} cross-linked Alg polymer network in PBS due to the ion exchange.[54]

3.4. In Vitro Biological Properties of GelMA/Alg/CNC Hydrogels. For tissue regeneration applications, living cells are either seeded on hydrogel scaffolds after scaffold fabrication or encapsulated in the struts of hydrogel scaffolds during biofabrication of cell-laden scaffolds.[55,56] After construction through either route, the subsequent investigation of the in vitro biological performance of hydrogel scaffolds is essential. In the current study, hDPSCs were used to study the biocompatibility of GelMA/Alg/CNC hydrogels. Figure 10A shows the live/dead staining results of hDPSCs cultured on double cross-linked GelMA/Alg/CNC hydrogels after culturing for 24 and 72 h, respectively. hDPSCs were well-attached to the hydrogel surface after 24 h of culture, and more living hDPSCs were observed after 72 h of culture. The results of cell proliferation experiments shown in Figure 10B indicated that GelMA/Alg/CNC hydrogels with a high CNC content and a low Alg content, i.e., GelMA-0A5C, GelMA-1A4C, and GelMA-2A3C hydrogels, provided higher cell proliferation rates. It is well-known that Alg has intrinsic limitations for cell

https://doi.org/10.1021/acsomega.4c06458
ACS Omega 2024, 9, 48361−48373

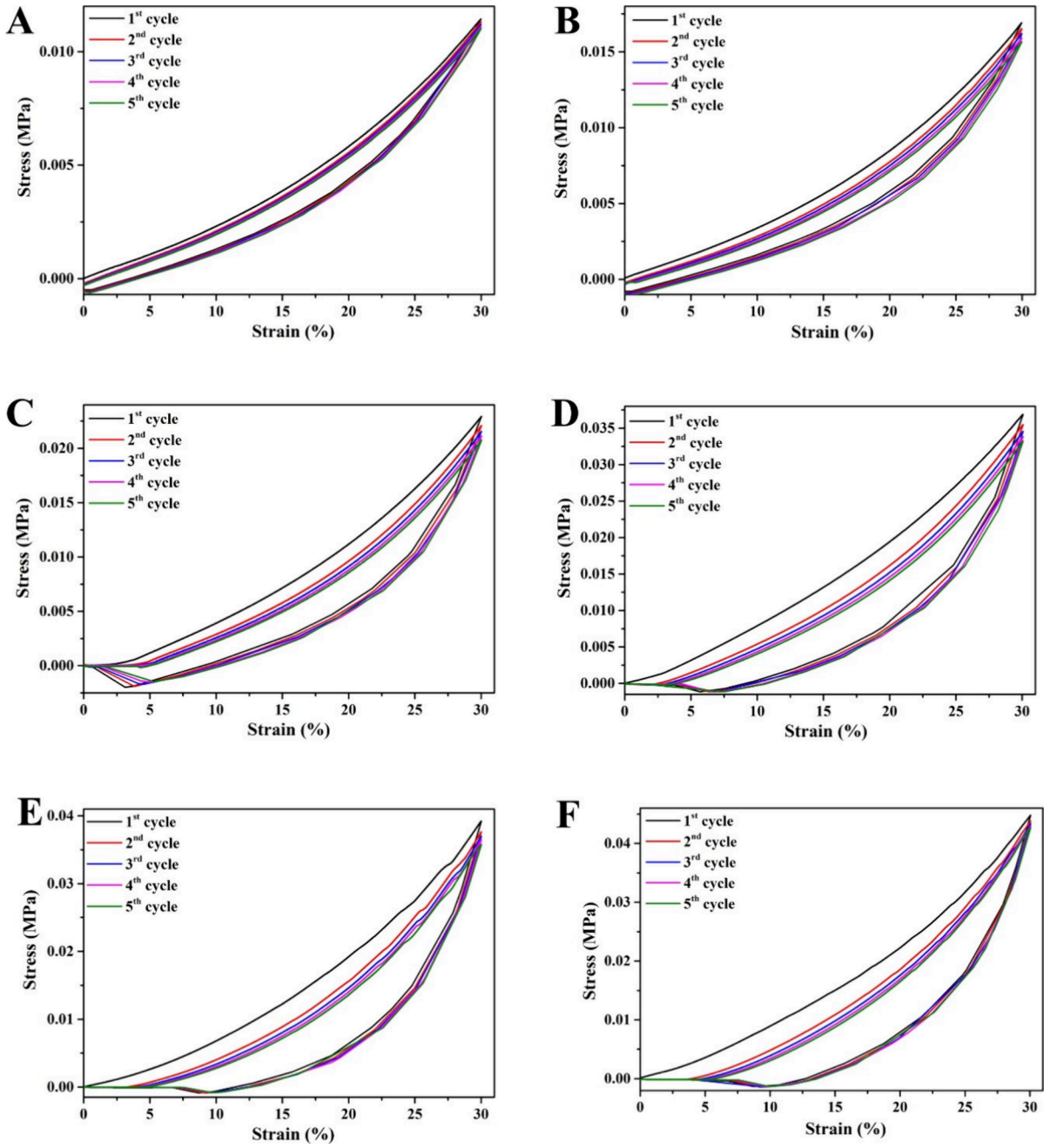

Figure 8. Cyclic compression behavior of GelMA/Alg/CNC hydrogels for a compression strain of 30%, with cyclic compression stress−strain curves of (A) GelMA-0A5C, (B) GelMA-1A4C, (C) GelMA-2A3C, (D) GelMA-3A2C, (E) GelMA-4A1C, and (F) GelMA-5A0C.

adhesion because of its inertness and lack of active sites for cell binding and interactions.[57,58] The results of in vitro biological investigations using hDPSCs have shown that GelMA/Alg/CNC hydrogels have the potential for dental tissue engineering applications. Although GelMA/Alg/CNC hydrogels exhibited low mechanical strength in comparison with conventional ceramics-based porous scaffolds for dental tissue engineering, the main benefits of using them are that GelMA/Alg/CNC hydrogels could encapsulate cells, such as hDPSCs, in the scaffolds for their delivery to the defect sites and that 3D printing technologies could produce personalized scaffolds for patients according to the size and geometry of tissue defects. Our future studies will focus on more in vitro investigations, as well as in vivo investigations, of 3D-printed GelMA/Alg/CNC hydrogels. Furthermore, bioprinting of hDPSC-laden GelMA/Alg/CNC hydrogels will be explored.

4. CONCLUSIONS

For fabricating hydrogel tissue engineering scaffolds via extrusion-based 3D printing, GelMA/Alg/CNC printing inks with different Alg:CNC ratios were designed and formulated to overcome the drawbacks of GelMA inks. GelMA, with good thermal-responsive behavior and photocurable ability, could be successfully synthesized in PBS. A high CNC content in inks could improve the printability of GelMA/Alg/CNC inks and simultaneously enhance the fidelity of the 3D-printed hydrogels. A high Alg content in inks could improve the mechanical strength of GelMA/Alg/CNC hydrogels due to the increased

https://doi.org/10.1021/acsomega.4c06458
ACS Omega 2024, 9, 48361−48373

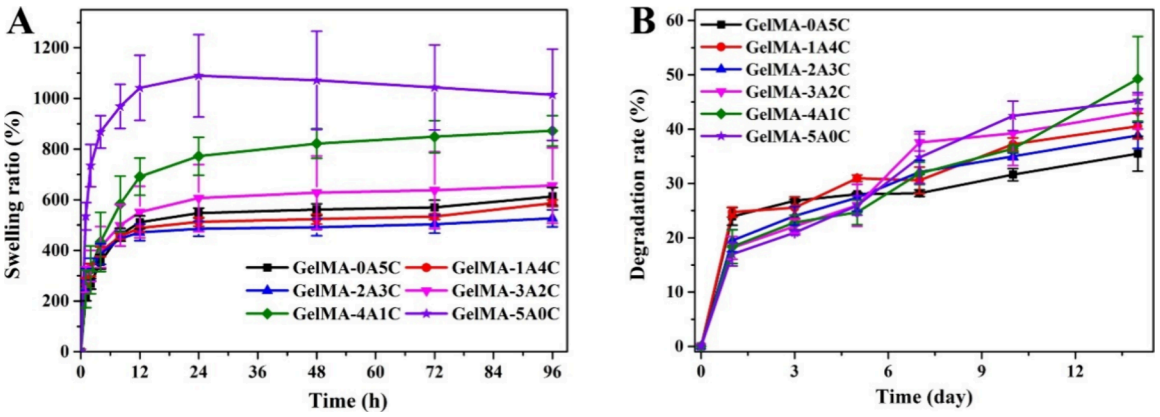

Figure 9. (A) Swelling behavior and (B) in vitro degradation behavior of GelMA/Alg/CNC hydrogels.

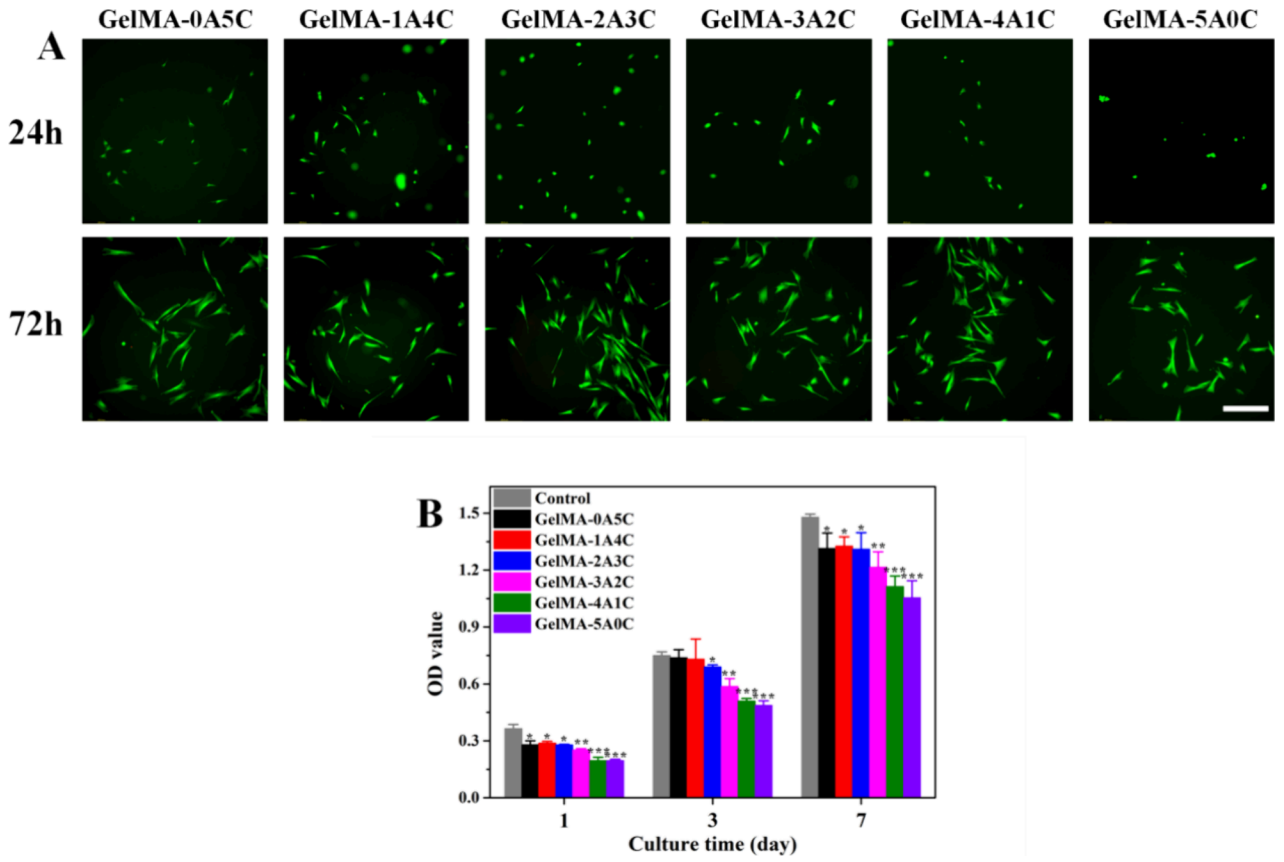

Figure 10. In vitro biological performance of GelMA/Alg/CNC hydrogels. (A) Fluorescence images of hDPSCs (green: live; red: dead) cultured on GelMA/Alg/CNC hydrogels for 24 and 72 h. Scale bar: 200 μm. (B) Cell proliferation of hDPSCs on GelMA/Alg/CNC hydrogels.

cross-linking density. Furthermore, GelMA/Alg/CNC hydrogels with a higher Alg content had a higher swelling ratio and degradation rate. GelMA/Alg/CNC hydrogels were highly elastic and exhibited excellent biocompatibility. GelMA/Alg/CNC hydrogels with a suitable Alg:CNC ratio exhibited the highest hDPSC proliferation rate. Overall, 3D-printed GelMA/Alg/CNC hydrogels have potential for applications in dental tissue engineering.

AUTHOR INFORMATION

Corresponding Authors

Waruna Lakmal Dissanayaka − *Applied Oral Sciences & Community Dental Care, Faculty of Dentistry, Prince Philip Dental Hospital, The University of Hong Kong, Hong Kong,* orcid.org/0000-0002-3621-4866; Email: warunad@hku.hk

Min Wang − *Department of Mechanical Engineering Faculty of Engineering, The University of Hong Kong, Hong Kong, Hong Kong;* orcid.org/0000-0002-6495-5637; Email: memwang@hku.hk

Authors

Huihua Li − *Applied Oral Sciences & Community Dental Care, Faculty of Dentistry, Prince Philip Dental Hospital, The University of Hong Kong, Hong Kong, Hong Kong;* orcid.org/0000-0002-4272-4248

https://doi.org/10.1021/acsomega.4c06458
ACS Omega 2024, 9, 48361−48373

Shangsi Chen − *Department of Mechanical Engineering Faculty of Engineering, The University of Hong Kong, Hong Kong, Hong Kong*

Complete contact information is available at: https://pubs.acs.org/10.1021/acsomega.4c06458

Author Contributions

H.L.: design of research, methodology, investigation, and writing; S.C.: methodology, investigation, and writing; W.L.D.: research funding, design of research, research supervision, writing, reviewing, and editing; M.W.: research funding, design of research, research supervision, writing, reviewing, and editing. H.L. and S.C. contributed equally to this work.

Notes

The authors declare no competing financial interest.

■ ACKNOWLEDGMENTS

W.L.D. thanks the financial support received by the Research Grants Council (RGC), Hong Kong, and Health and Medical Research Fund, Food and Health Bureau, Hong Kong, through research grants 17117619, 07183816, 17125421, and Seed Fund for Basic Research by The University of Hong Kong (HKU). M.W. thanks Hong Kong's RGC for the financial support for this work through research grants 17200519, 17202921, 17201622, N_HKU749/22, and 17201324 and also HKU for funding under the Seed Fund for Basic Research Scheme. Assistance provided by members of W.L.D.'s and M.W.'s research groups and by technical staff in HKU's Department of Mechanical Engineering, Faculty of Dentistry, and Electron Microscopy Unit is acknowledged.

■ REFERENCES

(1) Forbes, S. J.; Rosenthal, N. Preparing the ground for tissue regeneration: from mechanism to therapy. *Nat. Med.* **2014**, *20* (8), 857−869.

(2) Kang, H. W.; Lee, S. J.; Ko, I. K.; Kengla, C.; Yoo, J. J.; Atala, A. A 3D bioprinting system to produce human-scale tissue constructs with structural integrity. *Nat. Biotechnol.* **2016**, *34* (3), 312−319.

(3) Kim, D. M.; Shin, M. J.; Kim, H.; Park, D.; Jeon, I. H.; Kholinne, E.; Koh, K. H. Comparison between autografts and allografts in superior capsular reconstruction: a systematic review of outcomes. *Orthop. J. Sports Med.* **2020**, *8* (3), No. 2325967120904937.

(4) Ji, W.; Hou, B.; Lin, W.; Wang, L.; Zheng, W.; Li, W.; Zheng, J.; Wen, X.; He, P. 3D Bioprinting a human iPSC-derived MSC-loaded scaffold for repair of the uterine endometrium. *Acta Biomater.* **2020**, *116*, 268−284.

(5) Guo, J. L.; Kim, Y. S.; Mikos, A. G. Biomacromolecules for tissue engineering: emerging biomimetic strategies. *Biomacromolecules* **2019**, *20* (8), 2904−2912.

(6) Hoang, D. M.; Pham, P. T.; Bach, T. Q.; Ngo, A. T. L.; Nguyen, Q. T.; Phan, T. T. K.; Nguyen, G. H.; Le, P. T. T.; Hoang, V. T.; Forsyth, N. R.; Heke, M.; Nguyen, L. T. Stem cell-based therapy for human diseases. *Signal Transduct. Target. Ther.* **2022**, *7* (1), 272.

(7) Jiang, Z.; Diggle, B.; Tan, M. L.; Viktorova, J.; Bennett, C. W.; Connal, L. A. Extrusion 3D printing of polymeric materials with advanced properties. *Adv. Sci.* **2020**, *7* (17), No. 2001379.

(8) Saadi, M.; Maguire, A.; Pottackal, N. T.; Thakur, M. S. H.; Ikram, M. M.; Hart, A. J.; Ajayan, P. M.; Rahman, M. M. Direct ink writing: a 3D printing technology for diverse materials. *Adv. Mater.* **2022**, *34* (28), No. 2108855.

(9) Jiang, G.; Li, S.; Yu, K.; He, B.; Hong, J.; Xu, T.; Meng, J.; Ye, C.; Chen, Y.; Shi, Z.; Feng, G.; Chen, W.; Yan, S.; He, Y.; Yan, R. A 3D-printed PRPGelMA hydrogel promotes osteochondral regeneration through M2 macrophage polarization in a rabbit model. *Acta Biomater* **2021**, *128*, 150−162.

(10) Hwangbo, H.; Lee, H.; Jin, E. J.; Lee, J.; Jo, Y.; Ryu, D.; Kim, G. Bio-printing of aligned GelMa-based cell-laden structure for muscle tissue regeneration. *Bioact Mater.* **2022**, *8*, 57−70.

(11) Ganguly, K.; Dutta, S. D.; Randhawa, A.; Patel, D. K.; Patil, T. V.; Lim, K. T. Transcriptomic changes toward osteogenic differentiation of mesenchymal stem cells on 3D-printed GelMA/CNC hydrogel under pulsatile pressure environment. *Adv. Healthcare Mater.* **2023**, *12* (11), No. 2202163.

(12) Ma, Y.; Xie, L.; Yang, B.; Tian, W. Three-dimensional printing biotechnology for the regeneration of the tooth and tooth-supporting tissues. *Biotechnol. Bioeng.* **2019**, *116* (2), 452−468.

(13) Choi, D.; Qiu, M.; Hwang, Y. C.; Oh, W. M.; Koh, J. T.; Park, C.; Lee, B. N. The effects of 3-dimensional bioprinting calcium silicate cement/methacrylated gelatin scaffold on the proliferation and differentiation of human dental pulp stem cells. *Materials (Basel)* **2022**, *15* (6), 2170.

(14) Xu, W.; Molino, B. Z.; Cheng, F.; Molino, P. J.; Yue, Z.; Su, D.; Wang, X.; Willfor, S.; Xu, C.; Wallace, G. G. On low-concentration inks formulated by nanocellulose assisted with gelatin methacrylate (GelMA) for 3D printing toward wound healing application. *ACS Appl. Mater. Interfaces* **2019**, *11* (9), 8838−8848.

(15) Boularaoui, S.; Shanti, A.; Lanotte, M.; Luo, S.; Bawazir, S.; Lee, S.; Christoforou, N.; Khan, K. A.; Stefanini, C. Nanocomposite conductive bioinks based on low-concentration GelMA and MXene nanosheets/gold nanoparticles providing enhanced printability of functional skeletal muscle tissues. *ACS Biomater Sci. Eng.* **2021**, *7* (12), 5810−5822.

(16) Chen, S.; Wang, Y.; Lai, J.; Tan, S.; Wang, M. Structure and properties of gelatin methacryloyl (GelMA) synthesized in different reaction systems. *Biomacromolecules* **2023**, *24* (6), 2928−2941.

(17) Yin, J.; Yan, M.; Wang, Y.; Fu, J.; Suo, H. 3D bioprinting of low-concentration cell-laden gelatin methacrylate (GelMA) bioinks with a two-step cross-linking strategy. *ACS Appl. Mater. Interfaces* **2018**, *10* (8), 6849−6857.

(18) Rizwan, M.; Chan, S. W.; Comeau, P. A.; Willett, T. L.; Yim, E. K. F. Effect of sterilization treatment on mechanical properties, biodegradation, bioactivity and printability of GelMA hydrogels. *Biomed Mater.* **2020**, *15* (6), No. 065017.

(19) O'Connell, C. D.; Zhang, B.; Onofrillo, C.; Duchi, S.; Blanchard, R.; Quigley, A.; Bourke, J.; Gambhir, S.; Kapsa, R.; Di Bella, C.; Choong, P.; Wallace, G. G. Tailoring the mechanical properties of gelatin methacryloyl hydrogels through manipulation of the photocrosslinking conditions. *Soft Matter* **2018**, *14* (11), 2142−2151.

(20) Rastin, H.; Ormsby, R. T.; Atkins, G. J.; Losic, D. 3Dbioprinting of methylcellulose/gelatin-methacryloyl (MC/GelMA) bioink with high shape integrity. *ACS Appl. Bio Mater.* **2020**, *3* (3), 1815−1826.

(21) Da Silva, K.; Kumar, P.; van Vuuren, S. F.; Pillay, V.; Choonara, Y. E. Three-dimensional printability of an ECM-based gelatin methacryloyl (GelMA) biomaterial for potential neuroregeneration. *ACS Omega* **2021**, *6* (33), 21368−21383.

(22) Wu, Y.; Wenger, A.; Golzar, H.; Tang, X. S. 3D bioprinting of bicellular liver lobule-mimetic structures via microextrusion of cellulose nanocrystal-incorporated shear-thinning bioink. *Sci. Rep* **2020**, *10* (1), 20648.

(23) Fan, Y.; Yue, Z.; Lucarelli, E.; Wallace, G. G. Hybrid printing using cellulose nanocrystals reinforced GelMA/HAMA hydrogels for improved structural integration. *Adv. Healthcare Mater.* **2020**, *9* (24), No. 2001410.

(24) Hafezi, M.; Khorasani, S. N.; Khalili, S.; Neisiany, R. E. Self-healing interpenetrating network hydrogel based on GelMA/alginate/nano-clay. *Int. J. Biol. Macromol.* **2023**, *242*, No. 124962.

(25) Wei, Q.; Zhou, J.; An, Y.; Li, M.; Zhang, J.; Yang, S. Modification, 3D printing process and application of sodium alginate based hydrogels in soft tissue engineering: A review. *Int. J. Biol. Macromol.* **2023**, *232*, No. 123450.

(26) Munoz-Perez, E.; Perez-Valle, A.; Igartua, M.; Santos-Vizcaino, E.; Hernandez, R. M. High resolution and fidelity 3D printing of

Laponite and alginate ink hydrogels for tunable biomedical applications. *Biomater Adv.* **2023**, *149*, No. 213414.
(27) Seyedmahmoud, R.; Celebi-Saltik, B.; Barros, N.; Nasiri, R.; Banton, E.; Shamloo, A.; Ashammakhi, N.; Dokmeci, M. R.; Ahadian, S. Three-dimensional bioprinting of functional skeletal muscle tissueusing gelatin methacryloyl-alginate boinks. *Micromachines* **2019**, *10* (10), 679.
(28) Nichol, J. W.; Koshy, S. T.; Bae, H.; Hwang, C. M.; Yamanlar, S.; Khademhosseini, A. Cell-laden microengineered gelatin methacrylate hydrogels. *Biomaterials* **2010**, *31* (21), 5536−5544.
(29) Choi, Y. H.; Yeo, Y. H.; Lee, D. J.; Park, S. A.; Park, W. H. 3D bioprinting of cell-laden thermosensitive methylcellulose/nanosilicate composite hydrogels. *Cellulose* **2023**, *30* (8), 5093−5112.
(30) Ouyang, L.; Yao, R.; Zhao, Y.; Sun, W. Effect of bioink properties on printability and cell viability for 3D bioplotting of embryonic stem cells. *Biofabrication* **2016**, *8* (3), No. 035020.
(31) Rebers, L.; Reichsollner, R.; Regett, S.; Tovar, G. E. M.; Borchers, K.; Baudis, S.; Southan, A. Differentiation of physical and chemical cross-linking in gelatin methacryloyl hydrogels. *Sci. Rep* **2021**, *11* (1), 3256.
(32) Schuurman, W.; Levett, P. A.; Pot, M. W.; van Weeren, P. R.; Dhert, W. J.; Hutmacher, D. W.; Melchels, F. P.; Klein, T. J.; Malda, J. Gelatin-methacrylamide hydrogels as potential biomaterials for fabrication of tissue-engineered cartilage constructs. *Macromol. Biosci* **2013**, *13* (5), 551−561.
(33) Wang, X.; Ao, Q.; Tian, X.; Fan, J.; Tong, H.; Hou, W.; Bai, S. Gelatin-based hydrogels for organ 3D bioprinting. *Polymers* **2017**, *9* (9), 401.
(34) Messaoud, G. B.; Aveic, S.; Wachendoerfer, M.; Fischer, H.; Richtering, W. 3D printable gelatin methacryloyl (GelMA)-dextran aqueous two-phase system with tunable pores structure and size enables physiological behavior of embedded cells in vitro. *Small* **2023**, *19* (44), No. 2208089.
(35) Jo, S.; Lee, J.; Lee, H.; Ryu, D.; Kim, G. The one-step fabrication of porous hASC-laden GelMa constructs using a handheld printing system. *npj Regen. Med.* **2023**, *8* (1), 30.
(36) Outrequin, T. C. R.; Gamonpilas, C.; Siriwatwechakul, W.; Sreearunothai, P. Extrusion-based 3D printing of food biopolymers: A highlight on the important rheological parameters to reach printability. *J. Food Eng.* **2023**, *342*, No. 111371.
(37) Tagami, T.; Ito, E.; Kida, R.; Hirose, K.; Noda, T.; Ozeki, T. 3D printing of gummy drug formulations composed of gelatin and an HPMC-based hydrogel for pediatric use. *Int. J. Pharm.* **2021**, *594*, No. 120118.
(38) Sanchez-Sanchez, R.; Rodriguez-Rego, J. M.; Macias-Garcia, A.; Mendoza-Cerezo, L.; Diaz-Parralejo, A. Relationship between shear-thinning rheological properties of bioinks and bioprinting parameters. *Int. J. Bioprint.* **2023**, *9* (2), 687.
(39) Ansari, S.; Rashid, M. A. I.; Waghmare, P. R.; Nobes, D. S. Measurement of the flow behavior index of Newtonian and shear-thinning fluids via analysis of the flow velocity characteristics in a mini-channel. *Sn Appl. Sci.* **2020**, *2* (11), 1787.
(40) Occhetta, P.; Visone, R.; Russo, L.; Cipolla, L.; Moretti, M.; Rasponi, M. VA-086 methacrylate gelatine photopolymerizable hydrogels: A parametric study for highly biocompatible 3D cell embedding. *J. Biomed Mater. Res. A* **2015**, *103* (6), 2109−2117.
(41) Kyle, S.; Jessop, Z. M.; Al-Sabah, A.; Whitaker, I. S. 'Printability' of candidate biomaterials for extrusion based 3D printing: state-of-the-art. *Adv. Healthcare Mater.* **2017**, *6* (16), No. 1700264.
(42) Rodriguez-Rego, J. M.; Mendoza-Cerezo, L.; Macias-Garcia, A.; Mendoza-Cerezo, L.; Carrasco-Amador, J. P.; Marcos-Romero, A. C. Methodology for characterizing the printability of hydrogels. *Int. J. Bioprint.* **2023**, *9* (2), 667.
(43) Schwab, A.; Levato, R.; D'Este, M.; Piluso, S.; Eglin, D.; Malda, J. Printability and shape fidelity of bioinks in 3D bioprinting. *Chem. Rev.* **2020**, *120* (19), 11028−11055.
(44) Chen, S.; Li, J.; Zheng, L.; Huang, J.; Wang, M. Biomimicking trilayer scaffolds with controlled estradiol release for uterine tissue regeneration. *Exploration* **2024**, *4*, No. 20230141.
(45) Klar, V.; Pere, J.; Turpeinen, T.; Karki, P.; Orelma, H.; Kuosmanen, P. Shape fidelity and structure of 3D printed high consistency nanocellulose. *Sci. Rep* **2019**, *9* (1), 3822.
(46) Mora-Boza, A.; Wlodarczyk-Biegun, M. K.; Del Campo, A.; Vazquez-Lasa, B.; Roman, J. S. Glycerylphytate as an ionic crosslinker for 3D printing of multi-layered scaffolds with improved shape fidelity and biological features. *Biomater Sci.* **2020**, *8* (1), 506−516.
(47) Luo, Y.; Zhang, T.; Lin, X. 3D printed hydrogel scaffolds with macro pores and interconnected microchannel networks for tissue engineering vascularization. *Chem. Eng. J.* **2022**, *430*, No. 132926.
(48) Choi, Y. H.; Kim, S. H.; Kim, I. S.; Kim, K.; Kwon, S. K.; Hwang, N. S. Gelatin-based micro-hydrogel carrying genetically engineered human endothelial cells for neovascularization. *Acta Biomater* **2019**, *95*, 285−296.
(49) Rincón-Iglesias, M.; Lizundia, E.; Correia, D. M.; Costa, C. M.; Lanceros-Méndez, S. The role of CNC surface modification on the structural, thermal and electrical properties of poly(vinylidene fluoride) nanocomposites. *Cellulose* **2020**, *27* (7), 3821−3834.
(50) Jin, M.; Sun, N.; Weng, W.; Sang, Z.; Liu, T.; Xia, W.; Wang, S.; Sun, X.; Wang, T.; Li, H.; Yang, H. The effect of GelMA/alginate interpenetrating polymeric network hydrogel on the performance of porous zirconia matrix for bone regeneration applications. *Int. J. Biol. Macromol.* **2023**, *242*, No. 124820.
(51) Park, H.; Guo, X.; Temenoff, J. S.; Tabata, Y.; Caplan, A. I.; Kasper, F. K.; Mikos, A. G. Effect of swelling ratio of injectable hydrogel composites on chondrogenic differentiation of encapsulated rabbit marrow mesenchymal stem cells in vitro. *Biomacromolecules* **2009**, *10* (3), 541−546.
(52) Chawla, D.; Kaur, T.; Joshi, A.; Singh, N. 3D bioprinted alginate-gelatin based scaffolds for soft tissue engineering. *Int. J. Biol. Macromol.* **2020**, *144*, 560−567.
(53) Piao, Y.; You, H.; Xu, T.; Bei, H. P.; Piwko, I. Z.; Kwan, Y. Y.; Zhao, X. Biomedical applications of gelatin methacryloyl hydrogels. *Eng. Regen* **2021**, *2*, 47−56.
(54) Kim, E.; Kim, M. H.; Song, J. H.; Kang, C.; Park, W. H. Dual crosslinkedalginate hydrogels by riboflavin as photoinitiator. *Int. J. Biol. Macromol.* **2020**, *154*, 989−998.
(55) Gunther, M. I.; Weidner, N.; Muller, R.; Blesch, A. Cell-seeded alginate hydrogel scaffolds promote directed linear axonal regeneration in the injured rat spinal cord. *Acta Biomater* **2015**, *27*, 140−150.
(56) Yang, J.; Zhang, Y. S.; Yue, K.; Khademhosseini, A. Cell-laden hydrogels for osteochondral and cartilage tissue engineering. *Acta Biomater* **2017**, *57*, 1−25.
(57) Lin, Z.; Wu, M.; He, H.; Liang, Q.; Hu, C.; Zeng, Z.; Cheng, D.; Wang, G.; Chen, D.; Pan, H.; Ruan, C. 3D printingof mechanically stable calcium-free alginate-based scaffolds with tunable surface charge to enable cell adhesion and facile biofunctionalization. *Adv. Funct Mater.* **2019**, *29* (9), No. 1808439.
(58) Augst, A. D.; Kong, H. J.; Mooney, D. J. Alginate hydrogels as biomaterials. *Macromol. Biosci* **2006**, *6* (8), 623−633.

https://doi.org/10.1021/acsomega.4c06458
ACS Omega 2024, 9, 48361−48373